

Moreover, the cell wall can be considered as an effective and cheap scaffold for the deposition of nanomaterials with practical application in microelectronic devices such as electronic conductive microbridges and electrochemical biosensors.<sup>5</sup>

It was found, for example, that immobilization of hydrophilic oxidized carbon nanotubes onto the oppositely charged polyelectrolyte-coated yeast cells indicates that the polyelectrolyte/nanotube coating affects the electron mediation between yeast cells and an artificial electron acceptor.<sup>6</sup> This effect has been used to distinguish living and dead cells in various tests.

Among nanostructured carbon materials, we focused our attention on graphene because of its high electrical and mechanical properties and large surface area.<sup>7</sup> Interfacing living cells with graphene has been proven to be useful for the integration of cellular physiology with electrical readouts.<sup>8</sup> In the past, several studies reported the interaction of the edges of graphene sheets with the cell wall membrane,<sup>9</sup> the generation of reactive oxygen species by graphene,<sup>10</sup> and the trapping of living cells within graphene sheets.<sup>11</sup> Most recently, Kempaiah et al<sup>12</sup> encapsulated yeast cells with hard shells of graphene sheets, leading to enhanced protection of the cells from osmotic stresses and improving their stability, while Yang et al.<sup>13</sup> formed a nanosheet of graphene oxide on individual yeast cells by selectively depositing graphene oxide via layer-by-layer self-assembly.

These previous attempts considered abiotic processes, where coupling between the inorganic phase and living cell was obtained by chemical methods; here we propose a novel biogenic technique that exploits the ability of a microorganism to digest nutrients and use the byproduct as coupling agents with the inorganic phase. *Saccharomyces cerevisiae* (SaC) is a type of yeast widely used in the conversion of sugar and starch-based substrate into ethanol because of its ability to produce high amounts of ethanol and glucose as byproducts.<sup>14,15</sup> Moreover, in brewer yeast fermentation flocculation commonly occurs when the sources of fermentable sugars are exhausted.<sup>16</sup> During flocculation, the yeast cells aggregate rapidly in the medium in which they are suspended, forming a film after removal of the liquid medium.

In this paper, we report a method where the production of glucose during SaC fermentation was used to couple graphene nanoplatelets (GNPs) onto the yeast cell wall and, when sugar is exhausted, to obtain composite films with synergetic mechanical and electrical properties. Finally, from this fermentation process, in the presence of a nutrient material, i.e., sucrose, the yeast cells trigger the graphene assembly that is used to self-repair the mechanically damaged composite.

For preparation of the composite film, 40 mg of GNPs (purchased from Cheaptubes; thickness 8–15 nm) was dispersed for 3 h at room temperature in 40 mL of water using a sonication bath. A SaC-based commercial beer yeast extract with additives was used as the medium for fermentation. The dispersion of GNPs (1 mg/mL) was then added to the yeast solution and stirred at 110 rpm at 30 °C for 1 h. To start the fermentation, sugar (i.e., sucrose, 4 g) was added to the yeast/GNPs solution. The dispersion was heated at 35 °C to allow the fermentation process to proceed. The solid films were obtained by evaporating the water in excess, leaving the solutions in a sterilized silicon rubber mold at 30 °C in an inert atmosphere for 2 nights. Field-emission scanning electron microscopy (FESEM) was used to investigate the cross sections of the samples obtained by fracture in liquid nitrogen. Ultraviolet–visible (UV–vis) measurements of the deposited films were carried out with a PerkinElmer spectrometer Lambda 35; for all samples, a neat quartz slide was used as the reference. The optical absorbance was obtained on films of the same thickness ( $\approx 5 \mu\text{m}$ ). The current–voltage ( $I - V$ ) characteristic was performed by a computer-controlled Keithley 4200 Source Measure Unit. The electrical conductivity of the samples was monitored, at room temperature, by applying a sweeping direct-current electric voltage across the sample. The photocurrent was recorded on the same samples as those prepared for the optical absorbance, under an AM1.5D 150 mW/cm<sup>2</sup> illumination source from a Thermal Oriel solar simulator. Photoelectrical measurements were obtained for the films over several on/off light illumination cycles.

FESEM was used to investigate the surfaces of the samples. Parts a and b of Figure 1

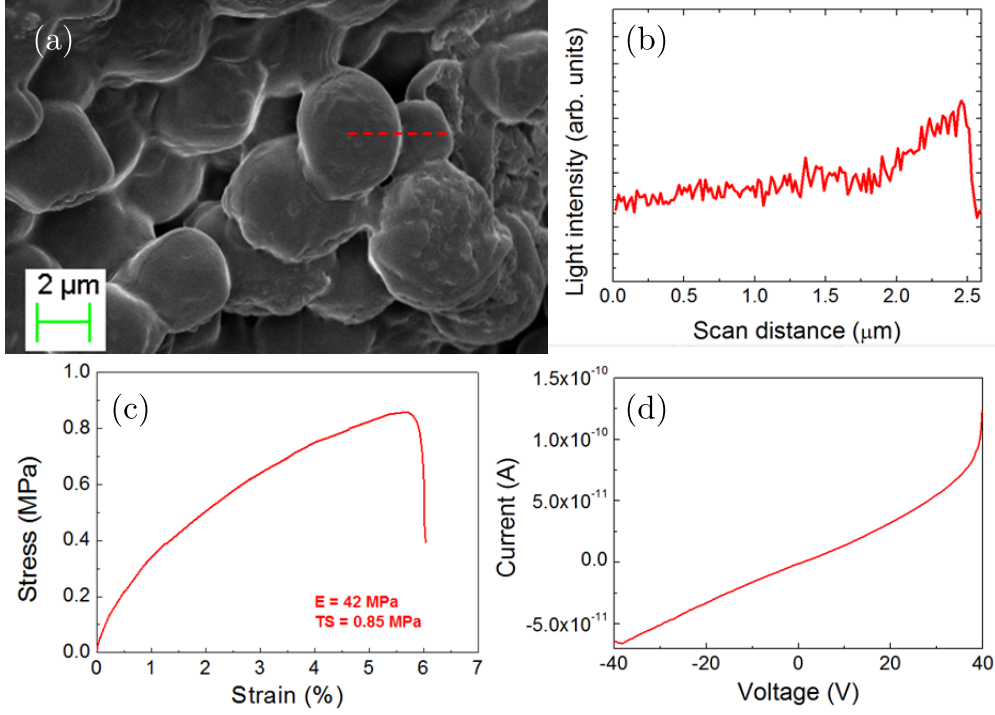


Figure 1: (a) FESEM image of the yeast cells. (b) Surface line scan. (c) Stress–strain curve of the plain yeast cell film. (d)  $I$ – $V$  characteristic of the yeast film.

show that the fermented yeast film mainly consist of whole cells and that the plain yeast cells do not exhibit surface features. The effect on the film morphology when GNPs were added during fermentation is reported in Figure 2. The line scan on the GNP/yeast cell surface indicates for the composite film the formation of wrinkles; these wrinkles arise from compressive stress when a soft-matter core (i.e., SaC yeast cell in our case) is coupled with a thin, high modulus sheet (i.e., GNPs).<sup>17</sup>

According to Cerda and Mahadevan,<sup>17</sup> in the case limit when the wavelength of the wrinkle is much lower than the substrate thickness and much higher than the skin thickness, the physics and geometry of such a system indicates that the wrinkle wavelength is given by:<sup>18,19</sup>

$$\lambda = 2\pi t \left[ \frac{(1 - \nu_s^2) E}{(1 - \nu^2) 3E_s} \right]^{1/3} \quad (1)$$

where  $t$  is the thickness of the GNP skin,  $E$  and  $\nu$  are respectively Young's modulus and Poisson's ratio of the skin, and  $E_s$  and  $\nu_s$  are respectively Young's modulus and Poisson's ratio

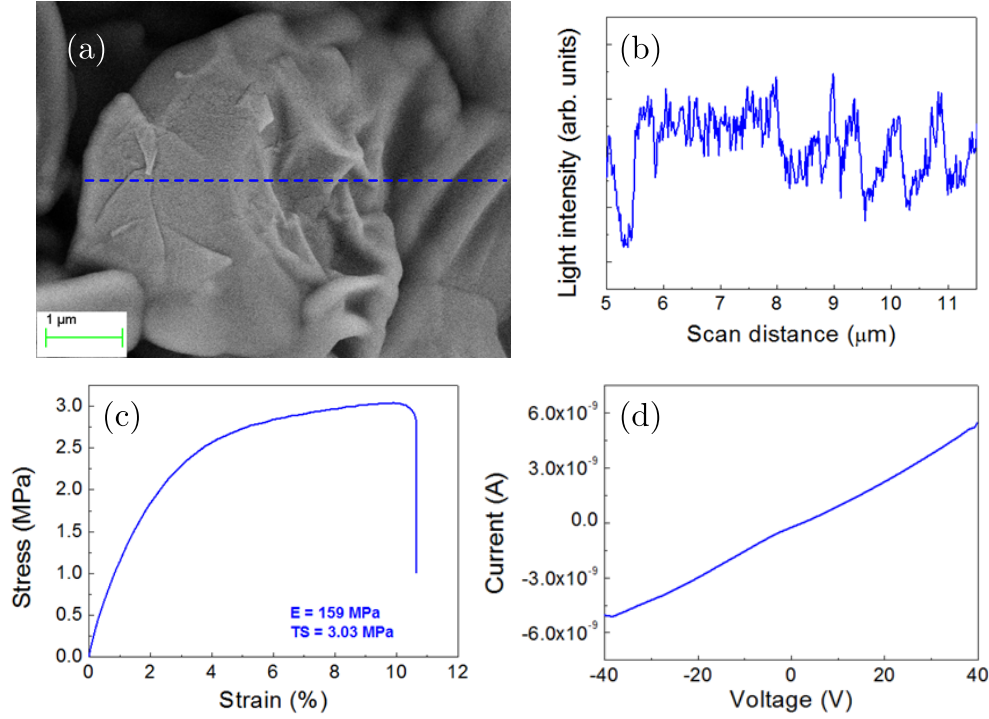


Figure 2: FESEM image of the GNPs/yeast cell. (b) Line scan of the surface showing wrinkles with a wavelength of about 30–70 nm. (c) Stress–strain curve of the undamaged composite film. (d)  $I$ – $V$  characteristic of the composite film.

of the substrate. Assuming an average thickness  $t = 11.5$  nm,  $E = 50$  GPa as determined below,  $\nu = 0.165$ ,<sup>20</sup>  $E = 112$  MPa,<sup>21,22</sup> and  $\nu = 0.5$ ,<sup>22</sup> a wrinkling wavelength  $\lambda = 38$  nm would be obtained. This result is in agreement with our experimental value of 30-70 nm reported in Figure 2b.

The tensile properties of films, i.e., Young’s modulus ( $E$ ) and failure strength ( $\sigma_f$ ), were then measured using a universal tensile testing machine (Lloyd Instruments LR30K) with a 50 N static load cell. The film samples were cut into strips (30 nm x 12 nm). The gauge length was 20 mm, and the extension rate was set at 2 mm/min.  $\sigma_f$  is determined as the peak stress in the measured stress–strain curve, while the Young’s modulus is evaluated as the secant between strains of 0.1% and 0.2%. The mechanical and electrical properties of the plain yeast film (Figure 1c-d) were found to be improved when the cell wall was coupled with GNPs (Figure 2c,d). Such results will be rationalized below according to a synergetic effect.

Light absorbance in the UV–vis range of the prepared samples is presented in Figure 3a.

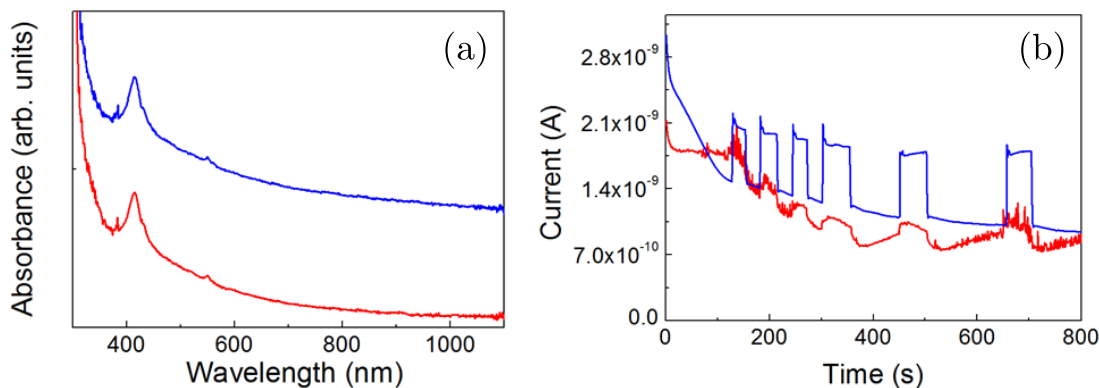


Figure 3: (a) UV-vis spectra of the yeast (red line) and composite (blue line) films, respectively. (b) Photocurrent recorded when the yeast (red line) and composite (blue line) films were exposed to illumination cycles. The change of the current intensity represents the switching on and off of the solar simulator.

In the visible range (350–800 nm), depending on the GNP incorporation, differences were obtained in terms of normalized optical absorbance. Figure 3b shows that a photocurrent signal was recorded on both samples. The spectral irradiance for a xenon lamp between 400 and 500 nm under the AM1.5D standard condition is about 16.9%; the absorption spectrum of the films in this optical window (i.e., 416 nm; Figure 3a) supports the observation that a photocurrent signal for the yeast can be recorded. This result is in accordance to that found by Hildebrandt et al.,<sup>23</sup> who recorded photocurrents and photovoltages with a yeast plasma membrane attached to a planar lipid membrane and to a poly(tetrafluoroethylene) (Teflon) film, respectively. It was found that the photoresponse, estimated as the relative variation between the dark and light signals, increases from 9% to 47% when the yeast film was compared with the composite film.

Mechanical stresses due to osmotic changes on the cell wall could represent a risk for the cell viability and membrane-transport activities. Self-repair is a common and wonderful phenomenon of living organisms to allow them to adapt to constantly changing environments. The main challenges in this regard are the development of nanostructured shells that do not disturb the cell proliferation and that, at the same time, are able to reassemble onto the cell surface when encapsulation is broken by an external harsh environment. Once shell structures

are broken, a decrease of the mechanical strength and a loss of functionality of encapsulated cells will occur. A way to self-repair the functional nanoscale shell is thus preferred, mainly if such nanoshells could self-assemble onto the cell surface during its proliferation. The repairing properties of our biohybrids are reported in Figure 4. After 30 min in the high-vacuum conditions of FESEM (Figure 4a), the presence of cracks on the surface of the cell is well visible and suggests that a strain could induce such an effect on GNP sheets. It could be reasonable that coupling between the GNP sheets and the cell wall hinders cell dehydration through its membrane, and the yeast cell would expand its volume via hypoosmotic shock. This straining effect is evident on the mechanical and electrical characteristics of the graphene-based composite, as reported in Figure 4c–e, where the decrease of the electrical conductivity as well as the reduction of the mechanical strength with respect to the unstressed composite film is attributed to the loss of the graphene connecting network.

We observed that such an effect is reversible upon placement of the composite film in the nutrient broth, i.e., an aqueous solution of sucrose and GNPs, for 40 min. As suggested by FESEM analysis (Figure 4b), the cracks almost disappear; the nutrient broth reconstructs the GNP shell, and the strain-induced effect on GNP sheets is canceled, with the mechanical strength and electrical conductivity being almost restored (Figures 4d–f).

The bionic composite shows remarkable improvements in the mechanical properties. Indeed, the undamaged composite has 3.5 times higher failure strength, and it is about 9 times tougher than the pristine yeast. Even the damaged film is able to guarantee an enhancement in performance, being 1.5 times stronger and showing an increase of toughness of +29%. After the self-repair, the composite is able to restore 85% of the undamaged composite strength and 83% of the toughness, thus showing a quite efficient healing mechanism.

The measured elastic and mechanical properties of the bionic composites, namely, the fracture strength  $\sigma_f$  and Young's modulus  $E$ , can be related to the properties of the constituent

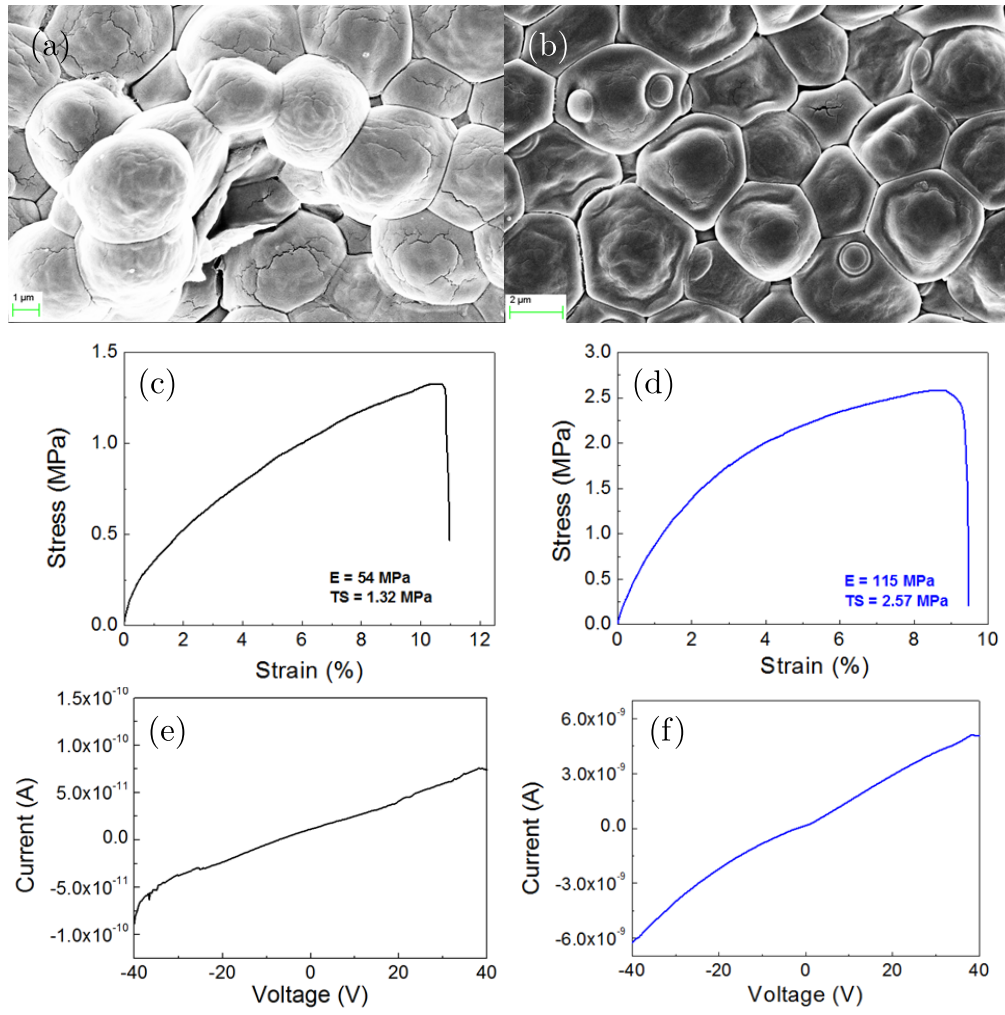


Figure 4: FESEM images, stress–strain curves, and  $I$ – $V$  characteristics of the damaged (a, c, and e) and repaired (b, d, and f) composite films, respectively.

phases via rules of mixture:

$$\sigma_f = f\sigma_{f\text{-GNP}} + (1 - f)\sigma_{f\text{-yeast}} \quad (2a)$$

$$E_f = fE_{f\text{-GNP}} + (1 - f)E_{f\text{-yeast}} \quad (2b)$$

where  $f$  is the volumetric fraction of the GNP film and the subscripts refer to each component of the bionic composite. A simple system of two fermented cells was modeled via Finite Element Method (FEM) simulations in order to understand the effect of the incorporation of GNPs. As operated in our work on yeast carbon nanotubes bionic composites,<sup>24</sup> the shape of the cells within the ensemble is approximated as hexagonal prism, starting from the actual cell arrangement in the ensemble (Figure 4b). The dimensions of the cells, mother and daughter, were taken from the work of Ahmad et al.<sup>25</sup> They reported for the mother cell a diameter  $d_m = 5.565 \mu\text{m}$  and for the daughter cell  $d_d = 4.467 \mu\text{m}$ . The cell dimension measurements from this work are consistent with our estimations.<sup>24</sup> The hexagonal base of the prism was dimensioned in order to have an area equivalent to a circle of diameter  $d$ , while the cell height was finally univocally determined from the cell volume also reported elsewhere.<sup>25</sup> Considering these geometrical characteristics for the cell, we obtain that  $f = 0.35 \%$  and  $0.18 \%$ , assuming limit values for the GNP film thicknesses of  $t_{\text{GNP,max}} = 15 \text{ nm}$  and  $t_{\text{GNP,min}} = 8 \text{ nm}$ . The corresponding average for  $t_{\text{GNP,av}} = 11.6 \text{ nm}$  is  $f = 0.25 \%$ . With regard to the yeast constitutive behavior, the curve obtained from the pristine yeast (Figure 1c) has been adopted as input for simulations, using an elastic material with finite strain capability. The same relationship was used for both the mother and daughter cells even if, nominally, a slight difference in the mechanical properties was reported,<sup>23</sup> with the latter being softer. Actually, the experimental stress–strain relationship can be considered an average of the two. The cells are modeled with underintegrated solid elements with spurious mode stabilization.<sup>26</sup> The load is applied as imposed displacements on the lateral face of the cells (Figure 5). The interface between the two cells was modeled via a cohesive-zone-model-based contact<sup>26</sup> for

which the force–separation curve was derived in a study by the authors and associated with an estimated fracture energy of  $G_{f\text{-yeast}} = 0.0193 \text{ N/m}$ .<sup>24</sup> The GNP film has been modeled with shell elements with a thickness of 11.5 nm, being the average of the expected film thickness. This corresponds to a total of 34 layers of graphene, each of them associated with a through-thickness integration point within the shell. Two half cells with a GNP film in between has been modeled in a sort of “sandwich” structure with periodic boundary conditions at the symmetry planes: by doing this, we simulate an infinite multilayer alternation of the yeast cell layer and GNP film (Figure 5). The constitutive behavior of graphene has been taken from Xu et al.,<sup>20</sup> operating a scaling on the failure strength of the curves there reported in order to best fit the experimental curves with simulations and thus have an estimate of the mechanical properties of GNPs. Perfect bonding was assumed at the interface between the GNPs film and cell wall, with the constitutive behavior of this interface being unknown.

Figure 4 shows a comparison between the curves derived from experiments and from simulated tensile tests on two cells. The overall trend is well comparable, and the mechanical parameters determined from the simulation best fit are comparable with the one estimated with rules of mixture (Table 1), confirming the synergetic interaction between the GNP film and yeast cells. Our back-analysis estimation for the GNP mechanical properties is consistent with the literature.<sup>27</sup> The fracture pattern within the graphene film is also depicted for increasing tension: a first appearance of diagonal cracks within graphene on the cell surface is followed by their coalescence in the correspondence of the interface between the two cells at which global failure of the composite occurs. This is qualitatively comparable with the SEM experimental images of Figure 4a,b, and as obtained for yeast–carbon nanotube composites,<sup>27</sup> global failure occurs because of interface rather than cell rupture.

In this paper, graphene sheets are used to encapsulate the yeast cells with the aid of SaC fermentation in the presence of sucrose. We demonstrate that graphene sheets form an electrically conductive layer on the yeast cells, developing a synergetic mechanical coupling with the cell. The described experimental method is also useful to prepare self-healable

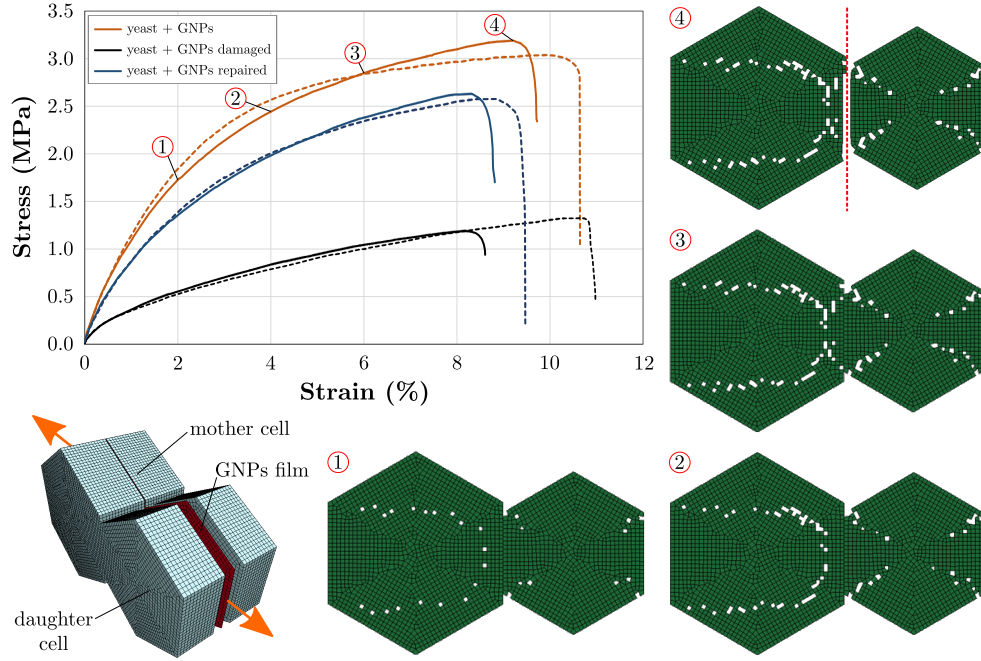


Figure 5: Simulation of the base “sandwich” composite element made up of a mother cell and a daughter cell with a GNP film in between of 11.5 nm thickness. The simulation-derived curves (continuous) are compared with the corresponding experimental counterpart (dashed). The evolution of the fracture pattern in the initially undamaged composite at four different states for increasing tension is depicted: composite failure occurs because of film rupture (state 4) along the interface between the two cells (compare with Figure 4b).

Table 1: (a) GNP properties determined from experiments through rules of mixture and from numerical simulations. The two values for the experimental estimates of the GNP properties come from the assumption of the GNP film limit thicknesses of  $t_{\text{GNP,max}} = 15$  nm and  $t_{\text{GNP,min}} = 8$  nm, respectively. For FEM simulations, an average thickness of  $t_{\text{GNP}} = 11.5$  nm is assumed.

| Material        | Experiments         |              |                                  |                           | FEM simulations     |              |                                  |                           |
|-----------------|---------------------|--------------|----------------------------------|---------------------------|---------------------|--------------|----------------------------------|---------------------------|
|                 | $\sigma_f$<br>[MPa] | $E$<br>[MPa] | $\sigma_{f,\text{GNP}}$<br>[MPa] | $E_{\text{GNP}}$<br>[GPa] | $\sigma_f$<br>[MPa] | $E$<br>[MPa] | $\sigma_{f,\text{GNP}}$<br>[MPa] | $E_{\text{GNP}}$<br>[GPa] |
| yeast+GNPs      | 3.1                 | 159          | 632–1185                         | 33.9–63.6                 | 3.2                 | 135          | 882                              | 50.1                      |
| yeast+GNPs dam. | 1.3                 | 54           | 136–255                          | 3.5–6.6                   | 1.2                 | 50           | 126                              | 5.3                       |
| yeast+GNP rep.  | 2.6                 | 115          | 500–937                          | 21.2–39.7                 | 2.6                 | 107          | 670                              | 31.7                      |

nanoshells that correlate the mechanical strain with the electrical readout. The possibility of distinguishing stressed cells is important for creating fast and cheap sensors for the detection of osmotic stress or testing nutrient adsorption on the cell wall. The method presented here may find a wide range of applications in bioelectronics and the development of novel materials.

## **Authors information**

### **Author contributions**

L.V. and N.M.P. had the idea, designed and supervised the entire research, and analyzed the results. S.B.B. prepared the samples and performed the characterizations. S.S. performed the FEM simulations. All authors have revised and given their approval to the final version of the manuscript.

### **Notes**

The authors declare no competing financial interest.

## **Acknowledgement**

N.M.P. is supported by the European Research Council (ERC StG Ideas 2011 BIHSNAM no. 279985 on “Bio-Inspired hierarchical supernanomaterials”, ERC PoC 2013 KNOTOUGH no. 632277 on “Supertough knotted fibers”, and ERC PoC 2015 SILKENE no. 693670 on “Bionic silk with graphene or other nanomaterials spun by silkworms”), by the European Commission under the Graphene Flagship (WP10 “Nanocomposites”, no. 604391), and by the Provincia Autonoma di Trento (“Graphene Nanocomposites”, no. S116/2012-242637 and delib. reg. no. 2266). S.S. acknowledges support from BIHSNAM.

## References

- (1) Xia, F.; Jiang, L. Bio-Inspired, Smart, Multiscale Interfacial Materials. *Adv. Mater.* **2008**, *20*, 2842.
- (2) Yang, S. H.; Ko, E. H.; Jung, Y. H.; Choi, I. S. Bioinspired Functionalization of Silica-Encapsulated Yeast Cells. *Angew. Chem., Int. Ed.* **2011**, *50*, 6115.
- (3) Wang, B.; Liu, P.; Jiang, W. G.; Pan, H. H.; Xu, X. R.; Tang, R. K. Yeast Cells with an Artificial Mineral Shell: Protection and Modification of Living Cells by Biomimetic Mineralization. *Angew. Chem., Int. Ed.* **2008**, *47*, 3560.
- (4) Fakhrullin, R. F.; Minullina, R. T. Hybrid Cellular-Inorganic Core-Shell Microparticles: Encapsulation of Individual Living Cells in Calcium Carbonate Microshells. *Langmuir* **2009**, *25*, 6617.
- (5) Berry, V.; Rangaswamy, S.; Saraf, R. F. Highly Selective, Electrically Conductive Monolayer of Nanoparticles on Live Bacteria. *Nano Lett.* **2004**, *4*, 939.
- (6) Zamaleeva, A. I.; Sharipova, I. R.; Porfireva, A. V.; Evtugyn, G. A.; Fakhrullin, R. F. Polyelectrolyte-Mediated Assembly of Multiwalled Carbon Nanotubes on Living Yeast Cells. *Langmuir* **2010**, *26*, 2671.
- (7) Novoselov, K. S.; Geim, A. K.; Morozov, S. V.; Jiang, D.; Zhang, Y.; Dubonos, S. V.; Grigorieva, I. V.; Firsov, A. A. Electric Field Effect in Atomically Thin Carbon Films. *Science* **2004**, *306*, 666.
- (8) Kempaiah, R.; Chung, A.; Maheshwari, V. Graphene as Cellular Interface: Electromechanical Coupling with Cells. *ACS Nano* **2011**, *5*, 6025.
- (9) Akhavan, O.; Ghaderi, E. Toxicity of Graphene and Graphene Oxide Nanowalls Against Bacteria. *ACS Nano* **2010**, *4*, 5731.

- (10) Zhang, Y.; Ali, S. F.; Dervishi, E.; Xu, Y.; Li, Z.; Casciano, D.; Biris, A. S. Cytotoxicity Effects of Graphene and Single-Wall Carbon Nanotubes in Neural Phaeochromocytoma-Derived PC12 Cells. *ACS Nano* **2010**, *4*, 3181.
- (11) Akhavan, O.; Ghaderi, E.; Esfandiari, A. Wrapping Bacteria by Graphene Nanosheets for Isolation from Environment, Reactivation by Sonication and Inactivation by Near-Infrared Irradiation. *J. Phys. Chem. B* **2011**, *115*, 6279.
- (12) Kempaiah, R.; Salgado, S.; Chung, W. L.; Maheshwari, V. Graphene as Membrane for Encapsulation of Yeast Cells: Protective and Electrically Conducting. *Chem. Commun.* **2011**, *47*, 11480.
- (13) Yang, S. H.; Lee, T.; Seo, E.; Ko, E. H.; Choi, I. S.; Kim, B.-S. Interfacing Living Yeast Cells with Graphene Oxide Nanosheets. *Macromol. Biosci.* **2012**, *12*, 61.
- (14) Balat, M.; Balat, H.; Öz, C. Progress in Bioethanol Processing. *Prog. Energy Combust. Sci.* **2008**, *34*, 551.
- (15) Prijambada, I. D.; Hidayat, C.; Widiyanto, D. Selection of Yeast Strains for Ethanol Fermentation of Glucose-Fructose-Sucrose Mixture. *Indonesian Journal of Biotechnology* **2012**, *17*, 114.
- (16) Kourkoutas, Y.; Bekatorou, A.; Banat, I. M.; Marchant, R.; Koutinas, A. A. Immobilization Technologies and Support Materials Suitable in Alcohol Beverages Production: a Review. *Food Microbiol.* **2004**, *21*, 377.
- (17) Cerda, E.; Mahadevan, L. Geometry and Physics of Wrinkling. *Phys. Rev. Lett.* **2003**, *90*, 074302.
- (18) Whitesides, G. M.; Bowden, N.; Brittain, S.; Evans, A. G.; Hutchinson, J. W. Spontaneous formation of ordered structures in thin films of metals supported on an elastomeric polymer. *Nature* **1998**, *393*, 146.

- (19) Brojan, M.; Terwagne, D.; Lagrange, R.; Reis, P. M. Wrinkling Crystallography on Spherical Surfaces. *Proc. Natl. Acad. Sci. U. S. A.* **2015**, *112*, 14.
- (20) Xu, M.; Paci, T. J.; Oswald, J.; Belytschko, T. A Constitutive Equation for Graphene Based on Density Functional Theory. *Int. J. Solids Struct.* **2012**, *49*, 2582.
- (21) Smith, A. E.; Zhang, Z. B.; Thomas, C. R.; Moxham, K. E.; Middelberg, A. P. J. The Mechanical Properties of *Saccharomyces Cerevisiae*. *Proc. Natl. Acad. Sci. U. S. A.* **2000**, *97*, 9871.
- (22) Stenson, J. D. Investigating the Mechanical Properties of Yeast Cells. 2009.
- (23) Hildebrandt, V.; Fendler, K.; Heberle, J.; Hoffmann, A.; Bamberg, E.; Buldt, G. Bacteriorhodopsin Expressed in *Schizosaccharomyces-Pombe* Pumps Protons Through the Plasma-Membrane. *Proc. Natl. Acad. Sci. U. S. A.* **1993**, *90*, 3578.
- (24) Valentini, L.; Bon, S. B.; Signetti, S.; Tripathi, M.; Iacob, E.; Pugno, N. M. Fermentation Based Carbon Nanotube Multifunctional Bionic Composites. *Sci. Rep.* **2016**, *6*, 27301.
- (25) Ahmad, M. R.; Nakajima, M.; Kojima, S.; Homma, M.; Fukuda, T. In Situ Single Cell Mechanics Characterization of Yeast Cells Using Nanoneedles Inside Environmental SEM. *IEEE Trans. Nanotechnol.* **2008**, *7*, 607.
- (26) Belytschko, T.; Liu, W. K.; Moran, B.; Elkhodary, K. *Nonlinear Finite Elements for Continua and Structures*, 2nd ed.; John Wiley & Sons, 2013.
- (27) Dikin, D. A.; Stankovich, S.; Zimney, E. J.; Piner, R. D.; Dommett, G. H. B.; Evmenenko, G.; Nguyen, S. T.; Ruoff, R. S. Preparation and Characterization of Graphene Oxide Paper. *Nature* **2007**, *448*, 457.